An Introduction to the Probabilistic Linear Matching Method Framework for Structural Integrity Assessment Under Uncertain Design Conditions

Xiaoxiao Wang and Haofeng Chen

Abstract The novel probabilistic Linear Matching Method (pLMM) framework is developed by extending the current direct method, the Linear Matching Method (LMM), to deal with the probabilistic structural integrity assessment for engineering components under uncertain operating conditions. The pLMM framework covers several physics-based failure evaluation modules related to cyclic loads at elevated temperatures, including shakedown analysis, ratcheting analysis, low cycle fatigue (LCF) analysis and creep-fatigue analysis. To further improve the prediction efficiency, artificial neural network (ANN) technology is employed to build the data-driven surrogate relationship between the design parameters and the key responses regarding specified failure behaviour, with a series of probabilistic evaluation boundaries and assessment diagrams of engineering structures established to describe the uncertainty of the structural resistance. The reliability analysis techniques are involved as well, by which the failure probability is estimated considering the randomness of engineering problems. The pLMM framework is conducive to getting rid of the excessive dependence on the conventional safety factor with conspicuous conservativeness during risk management, enhancing the robustness of critical infrastructure.

1 Introduction

Structural integrity assessment provides a fundamental investigation of structural resistance against a certain failure mechanism by a series of deterministic experimental analyses and numerical simulations. To further reflect the uncertainty in the

X. Wang
Department of Mechanical & Aerospace Engineering, University of Strathclyde, James Weir Building, 75 Montrose Street, Glasgow G1 1XJ, UK

H. Chen (✉)
School of Mechanical and Power Engineering, East China University of Science and Technology, Shanghai 200237, China
e-mail: haofeng.chen@strath.ac.uk

G. Garcea and D. Weichert (eds.), *Direct Methods for Limit State of Materials and Structures*, Lecture Notes in Applied and Computational Mechanics 101,
https://doi.org/10.1007/978-3-031-29122-7_4

material properties, geometric parameters, boundary conditions and loads conditions of engineering infrastructures, the most commonly used strategy is to set an appropriate safety factor which is able to consider the adequate redundancy in the design process. [1–3]. Inevitably, this experience-based arbitrary decision-making may result in unreasonable conservativeness introduced due to the limited statistical information on the important structural responses. The feasible probabilistic structural integrity assessment technology contains two main prerequisites: the concise but accurate deterministic evaluation approach and the proper probabilistic analysis method, and integrating the two sections into a unified frame system is a challenging engineering problem to which enormous endeavour has been devoted in academia.

The case study of the reliability-based shakedown analysis for a high-pressure chamber is given out by Andrzej [4], where the shakedown analysis procedure (CYCLONE), Response Surface Method (RSM) and Monte Carlo Simulation (MCS) sampling method were adopted to address the randomness of the cyclic inner pressure and radius. Staat and Heitzer proposed a stochastic FEA procedure that is dedicated to implementing probabilistic shakedown analysis, and the benchmarks of the central holed plate, pipe junction and plate with mismatched weld and a crack were elaborated [5–7] and verified by related analytical studies.

The reduced-order model technique, as well as the surrogate model, is applicable to implicitly expressing the estimation of structural fatigue life [8, 9] under complicated operating environments with fewer computational resources. For instance, the artificial neural network (ANN) is widely applied to reliability-based fatigue evaluations [10], and the feedforward backpropagation multilayer perceptron (MLP) neural network was employed by Durodola [11], where the non-linear effect of mean stress on the fatigue life was examined in the probabilistic fatigue analysis. Another application was reported by Ref. [12], with the probabilistic fatigue damage of subsea pipe derived by the dynamic Bayesian network. A similar analysis scheme was also extended to investigate the probabilistic fatigue crack growth and propagation [13].

Concerning the components under the creep regime, Zhang [14] provided comparative research, where the abilities to predict the creep-fatigue life of 316 stainless steel of three neural networks were compared, revealing the superiority of physics-informed neural network for providing the creep-fatigue life approximation with better fitting quality. The machine learning-based creep-fatigue life prediction scheme of low-alloy steel 42CrMo4 specimen was constructed in Ref. [15], and the ANN-based damage model by the long short-term memory network and gated recurrent unit neural network was proved to be suitable for creep-fatigue life estimation under complicated conditions with non-linearly changing temperatures and mechanical strain rates.

Therefore, the plausible probabilistic analysis framework for structural integrity should satisfy the prerequisites in terms of three different levels. Firstly, the deterministic structural integrity evaluation program should keep a good balance between computational accuracy and efficiency. Next, the effective prediction model should be able to capture the pertinent nonlinear relationship between the design parameters and output, without depending on unaffordable computational resources. Finally, the

universal probabilistic analysis tool should be applicable for solving the structure-level problems, providing comprehensive statistical information and the failure risk.

The LMM procedures have been proven to be able to deal with a wide range of structural integrity assessments (as shown in Fig. 1) by adopting a series of linear calculation approaches to precisely match the structural non-linear responses, including shakedown analysis [16], ratcheting analysis [17], low cycle fatigue (LCF) analysis [18] and creep-fatigue analysis [19]. The LMM shakedown analysis procedure is developed to calculate the structural shakedown limit leveraging the time-independent residual stress [20], according to the upper bound shakedown theory. When tackling the load conditions leading to alternating plasticity, the structural plastic response and the related Low Cycle Fatigue (LCF) evaluations are able to be implemented by the Direct Steady Cycle Analysis (DSCA) procedure [21], with the varying residual stress determined iteratively. Based on the time-dependent residual stress field by the DSCA procedure, the LMM ratcheting analysis procedure is dedicated to assessing the structural resistance to progressive plastic behaviour, where the limit of the additional constant load condition is acquired [18]. In order to further take the creep effect into consideration during LCF analysis for high-temperature components, the latest extended Direct Steady Cycle Analysis (eDSCA) procedure [19], can analyse the creep-fatigue interaction in terms of both stress–strain response level and the damage level, providing an accurate prediction of the lifetime to creep-fatigue crack initiation.

In this study, the deterministic analysis procedures are extended to address the probabilistic assessment for engineering components under cyclic load conditions and elevated temperature, and the recent research benchmarks and engineering applications by means of the proposed pLMM methodology are delivered.

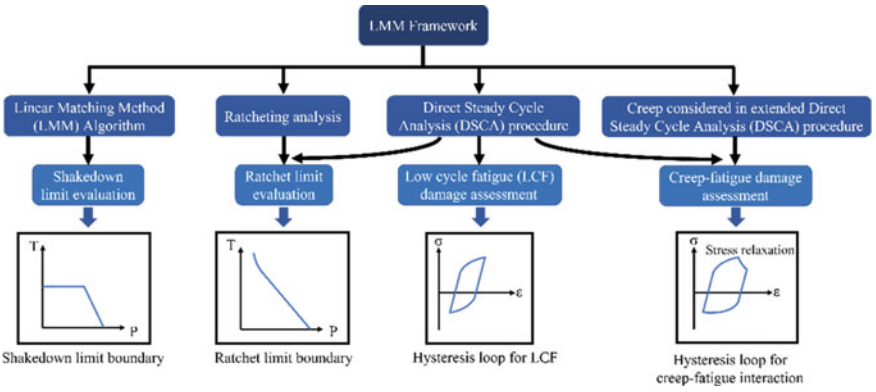

Fig. 1 Linear Matching Method (LMM) framework for structural integrity assessment regarding different failure mechanisms

2 Probabilistic Shakedown Analysis Under the pLMM Framework

2.1 *Probabilistic Shakedown Boundary and the Implementation of Reliability-Based Shakedown Analysis*

Establishment of the probabilistic shakedown boundary. The probabilistic shakedown boundary is conducive to visualizing the shakedown boundary affected by the uncertainty in design parameters, which can be built by implementing MCS samplings to estimate the statistical distribution of the LMM shakedown multipliers. As shown in Fig. 2, with the load ratio between Load 1 and Load 2, the envelope of probabilistic shakedown boundary and the associated statistical significance are displayed. And the failure risk against shakedown conditions raised by load conditions lying on the boundary is equal to the probability of the occurrence of the shakedown boundary.

Reliability-based shakedown analysis procedure. In order to perform the reliability-based shakedown evaluation and further examine the structural failure probability against shakedown conditions, a simplified governing function, the shakedown limit state indicator function (SLSIF), is expressed by Eq. (1) below.

$$G(\boldsymbol{X}) = \lambda(\boldsymbol{X}) - 1 \begin{cases} < 0, \text{Failed} \\ = 0, \text{ Limit state} \\ > 0, \text{Survival} \end{cases} \tag{1}$$

Here, the LMM shakedown multiplier λ functions as a state indicator, if the multiplier is equal to 1, it implies that the applied load condition lies on the shakedown boundary. A multiplier which is less than 1 always results in the current case working outside the shakedown boundary. On the other hand, for a survival case, the shakedown multiplier should be strictly guaranteed larger than the threshold value, $\lambda = 1$. The proposed

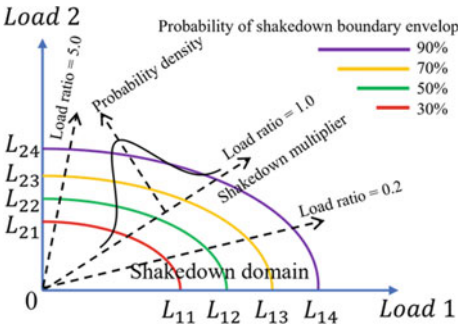

Fig. 2 Scheme of probabilistic shakedown boundary by different load ratios

SLSIF is then utilized directly by the First Order Reliability Method (FORM) [22] to acquire the structural failure probability and shakedown reliability index.

Description of deterministic FEA model. The benchmark of probabilistic shakedown analysis is demonstrated by the holed plate displayed in Fig. 3, which is discretized by the 20-node quadratic brick element C3D20R with reduced integration. And the ratio between the hole diameter D and the length L of the plate is 0.2, and the ratio between the depth d of the plate and the length L is equal to 0.05. Through the mesh convergence check, the total element number and minimum element size are determined to be 721 and 1.25 mm. Besides, Young's modulus E and the Poisson's ratio ν of the elastic-perfect plastic (EPP) material are assumed to be 2×10^5MPa and 0.3 respectively, and the material yield strength σ_y is defined to be 200MPa. The shakedown analysis is implemented considering the biaxial tensile load shown in Fig. 3, where the horizontal component P_1 is a constant uniform load and the vertical component P_2 is cyclic one. Detailed cyclic load pattern is depicted in Fig. 4.

Probabilistic shakedown boundary of the holed plate. Considering two random variables, the diameter of the central hole D and the material yield strength σ_y, the probabilistic shakedown boundaries of the holed plate are plotted in Fig. 5. This probabilistic shakedown assessment diagram is constructed by a series of random variables λ_i, and the statistical distributions of the LMM shakedown limit multiplier with different load ratios are displayed in Fig. 6. It is worth noting that the actual shakedown boundary should occur stochastically inside the envelope surrounded by a certain curve with corresponding probability.

Reliability-based shakedown analysis for the holed plate. According to the proposed shakedown limit state indicator function (SLSIF), the gradient vector of the SLSIF is generated during each iteration by calculating the convergent numerical partial derivatives of each random variable at the current design point. In the reliability-based shakedown analysis, there are two typical examples, with the

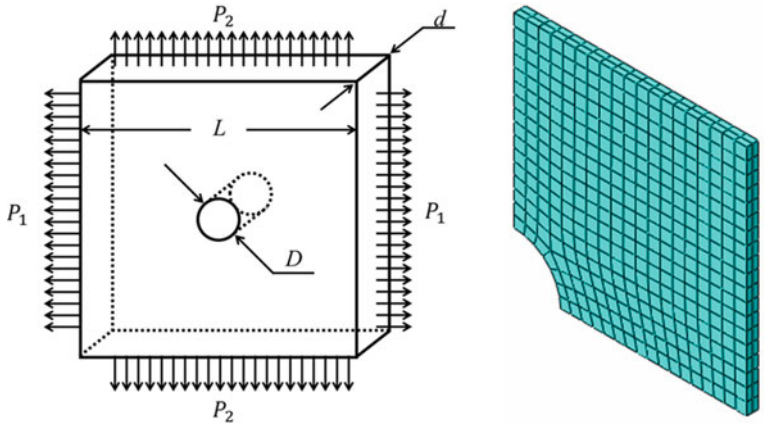

Fig. 3 FEA model of the central holed plate

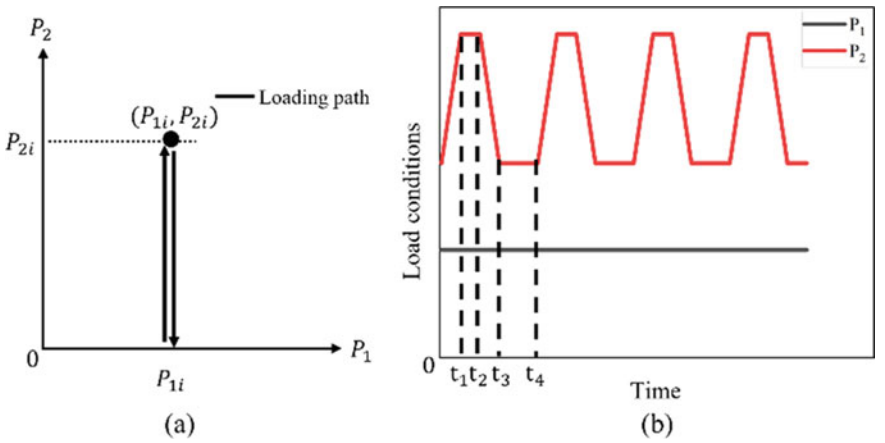

Fig. 4 Description of the time-dependent load conditions: **a** cyclic mode of the applied load path; **b** detailed spectrum of the applied load conditions

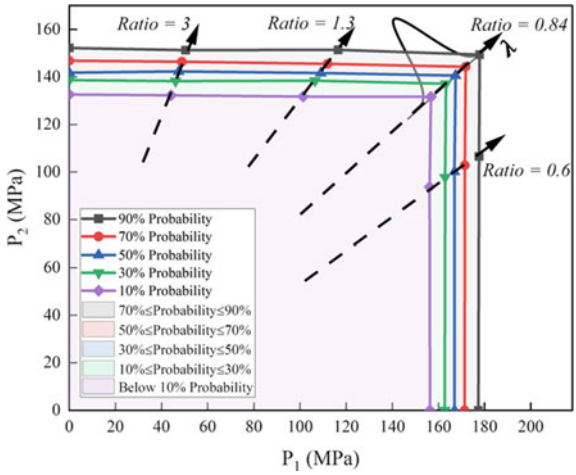

Fig. 5 Probabilistic shakedown boundaries of the central holed plate under predefined load path

load conditions on the deterministic shakedown boundary and inside the boundary involved (as shown in Fig. 7), respectively. The results of reliability analysis with different load conditions are listed in Table 1, and due to the uncertainties of geometric dimension and material property, even though the load condition (points 1 in Fig. 7) is located on the deterministic shakedown boundaries, the survival probability is only 70.45%, which is still much lower than 100%. The failure probability derived from pLMM-based reliability analysis is compared with the verifications with direct MCS, with all random variables remaining consistent with Table 1. The comparison shows that the results of the proposed probabilistic shakedown analysis are consistent with

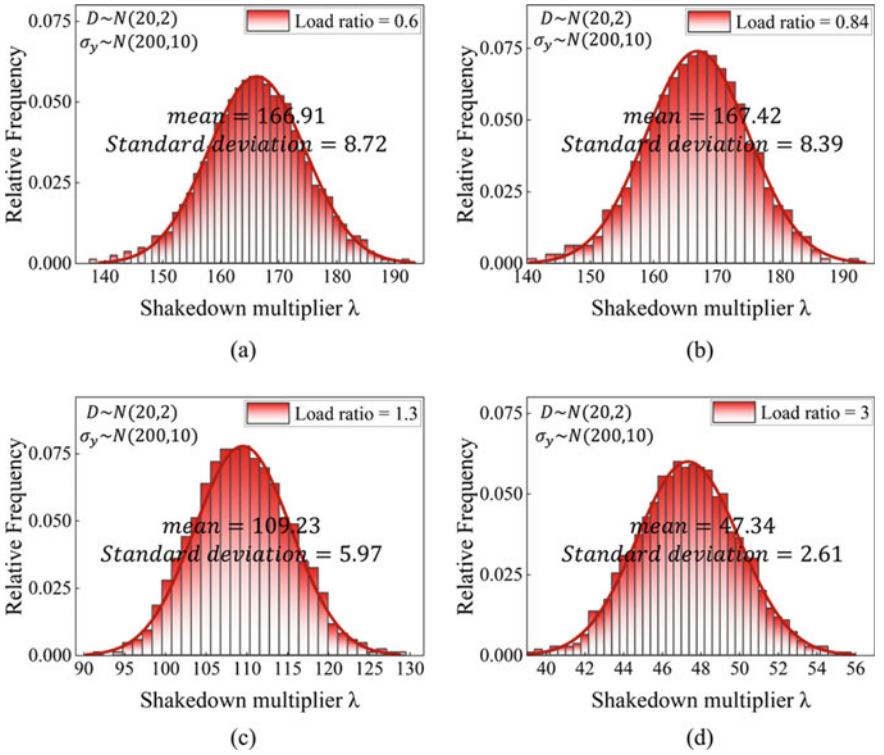

Fig. 6 Probabilistic distribution of LMM shakedown limit multiplier with different load ratios: **a** ratio = 0.6; **b** ratio = 0.84; **c** ratio = 1.3; **d** ratio = 3

the exact solutions provided by MCS (3,000 sampling points involved), with the relative error controlled within an acceptable range.

3 Probabilistic Low Cycle Fatigue and Ratcheting Analysis Under pLMM Framework

3.1 Linear Matching Method-Driven Neural Network (LDNN) for LCF Life and Ratchet Limit Predictions

The Linear Matching Method-driven neural network (LDNN) is built and employed as the multi-layer perceptron (MLP) for modelling and prediction [23], and the general network structure contains three layers: the input layer, the hidden layer and the output layer, as displayed in Fig. 8.

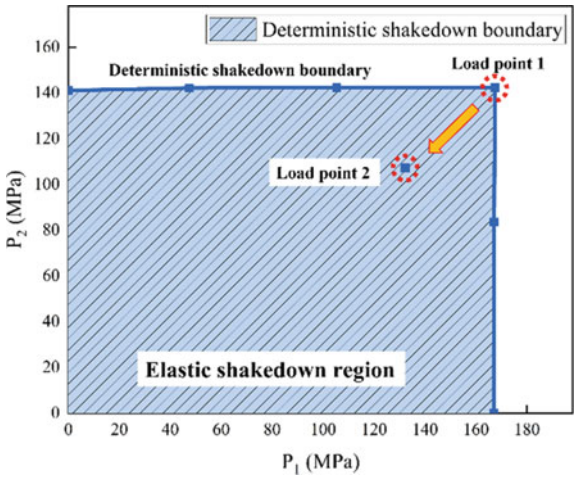

Fig. 7 Deterministic shakedown boundaries of the holed plate and the load conditions for reliability analyses

Table 1 Results of reliability-shakedown analysis by pLMM and the verifications with MCS

Load point index	Failure probability P_f	Verification by MCS	Error %
1	0.2954518037	0.2990909091	1.2167
2	0.04034325841	0.042962963	6.0976

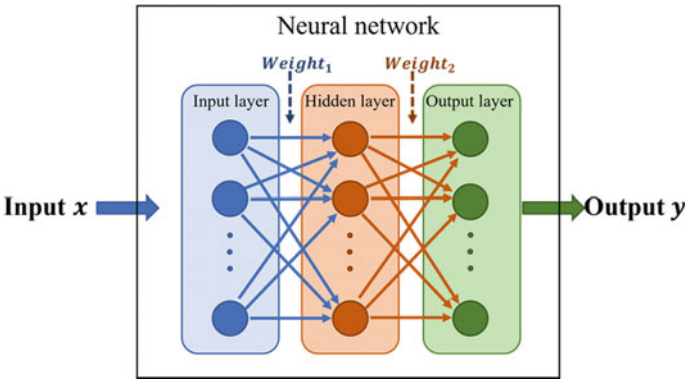

Fig. 8 General structure of a three-layer artificial neural network (ANN)

The data flow commences with the input data vector x passed in through the input layer to the hidden layer, during which the weight of each parameter is also added. Next, in the middle or hidden layer, the ellipsoidal basis function (EBF) [24] existing in each neuron plays the key role in the activation function, leading to the non-linear mapping process which is dependent on the summation of input with weights and bias. For implementing LCF lifetime and ratchet limit modelling, the interpolating

functions are formulated by Eqs. (2) and (3), where $\phi_i(x)$ is the basis function of EBF neural network [24], α_i and α_{N+1} are the weight and bias terms, respectively, and the L_f and λ represent the approximations of LCF life and ratchet limit multiplier.

$$L_f(\boldsymbol{x}) = \sum_{i=1}^{N} \alpha_i \phi_i(\boldsymbol{x}), \text{ for LCF lifetime modelling} \tag{2}$$

$$\lambda(\boldsymbol{x}) = \sum_{i=1}^{N} \alpha_i \phi_i(\boldsymbol{x}) + \alpha_{N+1}, \text{ for ratchet limit modelling} \tag{3}$$

The working flow of LDNN-based probabilistic LCF and ratcheting analyses under the pLMM framework is illustrated by three main steps included:

Step 1. Generating the training dataset by Latin Hypercube Sampling and processing the input dataset with LMM to acquire the structural response;

Step 2. Training [25] and testing the LMM-driven neural network (LDNN);

Step 3. Performing the probabilistic LCF or ratcheting analysis with surrogate models to predict the distribution of key output and the failure probability.

3.2 *Benchmark of Probabilistic Low Cycle Fatigue Analysis*

Description of the FEA model. To illustrate the applicability of the proposed probabilistic analysis scheme for LCF life assessment, a benchmark of the elbow pipe bend is investigated, and detailed descriptions of the geometry are given out in Fig. 9. Firstly, the structure of the elbow pipe bend is characterized by the dimension parameters in Table 2. The parameters R_O, t_n, R and L denote the outer radius of elbow pipe, nominal pipe wall thickness, bending radius and straight length, respectively. Besides, the bending characteristic, h, is defined as $Rt/{r_m}^2$, where r_m refers to the nominal mean radius of the pipe. The FEA model is discretized by ABAQUS, with the 20-node quadratic brick element C3D20R adopted, which keeps a good balance of numerical precision and computational efficiency by reduced integration technology. And inside the black dotted box, the elbow zone is refined so as to satisfy the requirements of mesh convergence and to capture the prominent stress gradient around this local region, with 4,760 elements created in total.

Adopted material properties and boundary conditions (BCs). The elbow pipe bend is made of austenitic stainless steel 316L, and the temperature-dependent material properties are provided [26] in Table 3, including Young's modulus E, Poisson's ratio ν, the average coefficient of linear thermal expansion α_m and thermal conductivity k. In addition, the temperature-dependent cyclic stress–strain relationship is described by Eqs. (4) and (5) in Ramberg–Osgood (R-O) form, where ε_{ta} is the total true strain amplitude, σ_a is the total true stress amplitude, $\overline{E}$ is the multi-axial Young's modulus, and K and n are the strength coefficient and plastic hardening parameters controlling the cyclic responses.

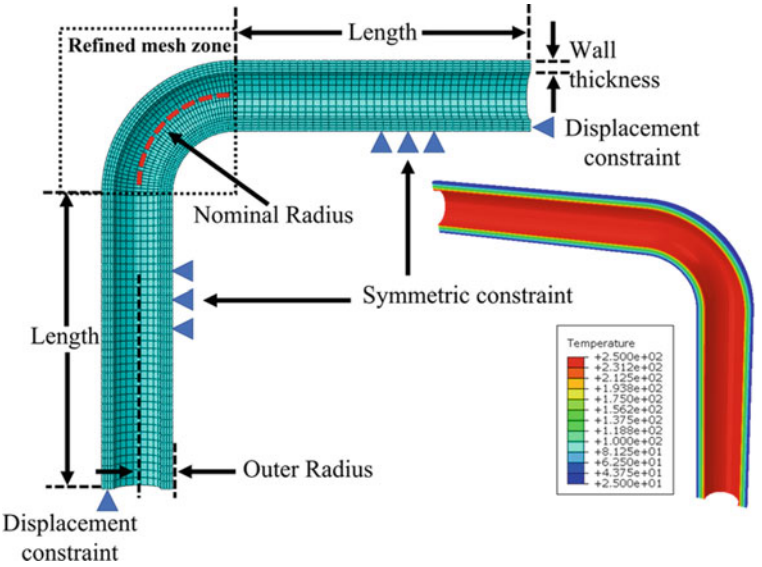

Fig. 9 Descriptions of the geometry and FEA model of the elbow pipe component for probabilistic LCF life and ratchet limit analyses

Table 2 Geometric dimensions of the elbow pipe bend

Outer radius $R_O(mm)$	Wall thickness $t_n(mm)$	Bending radius $R(mm)$	Length $L(mm)$	Bending characteristic h
180	60	500	1500	1.33

Table 3 Adopted temperature-dependent material properties of austenitic stainless steel 316L

Temperature (°C)	20	100	200	300	400
Young's modulus $E\left(10^3\text{MPa}\right)$	200	193	185	176	168
Poisson's ratio ν	0.3				
Coefficient of thermal expansion $\alpha_m\left(10^{-6}/°\text{C}\right)$	15.3	15.9	16.6	17.2	17.8
Thermal conductivity $k(\text{W/mm}\cdot\text{K})$	0.01428	0.01548	0.01698	0.01849	0.01999
K (MPa)	2286	2082	1860	1650	1650
n	0.351	0.339	0.325	0.31	0.31

$$\varepsilon_{ta} = \frac{\sigma_a}{\overline{E}} + \left(\frac{\sigma_a}{K}\right)^{\frac{1}{n}} \tag{4}$$

$$\overline{E} = \frac{3E}{2(1+v)} \tag{5}$$

The half model of the elbow pipe bend is created with the symmetric BCs exerted on the symmetric surfaces, and the displacement constraints are also applied along with the horizontal and vertical directions at each end of the elbow pipe, which are shown in Fig. 9. Besides, on the inner surfaces lies the constant inner pressure, and between the inner and outer surfaces of the pipe wall, there exists the cyclic temperature difference.

Deterministic ratchet limit boundary and alternating plastic response region. By means of the deterministic LMM procedures, the limit boundaries of the elbow pipe bend are established in Fig. 10, by which the structural responses are divided into two different sections: the ratcheting region and the reverse plasticity region. And the typical failure mechanisms in terms of LCF crack initiation and progressive plastic collapse (ratcheting) are compared in Fig. 11. Here, the horizontal and vertical coordinates are normalized by the limit load of the elbow pipe bend, 112.4MPa, and the applied reference temperature difference, 225°C, respectively.

Probabilistic LCF lifetime prediction by LDNN. Considering the uncertain design parameters, including the Material parameters K and n, Nominal thickness t_n, constant inner pressure P/P_0 and cyclic temperature difference $\Delta T/\Delta T_0$, the statistical distribution of the elbow pipe LCF life, visualized by the plots in Fig. 12, is investigated by employing the proposed LDNN-based surrogate model with 120 neuron pathways inside the hidden layer. Under the existence of random variables, including material property parameters (K and n), elbow pipe thickness and the inner pressure, the LCF life of elbow pipe bend tends to show the Lognormal distribution.

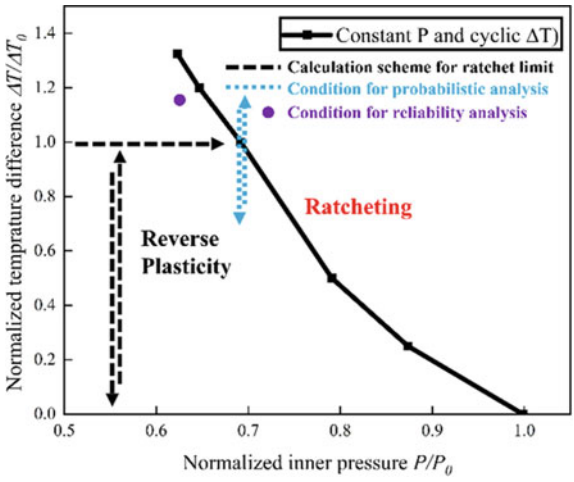

Fig. 10 Deterministic ratchet limit boundary and the reverse plasticity load region for the elbow pipe bend

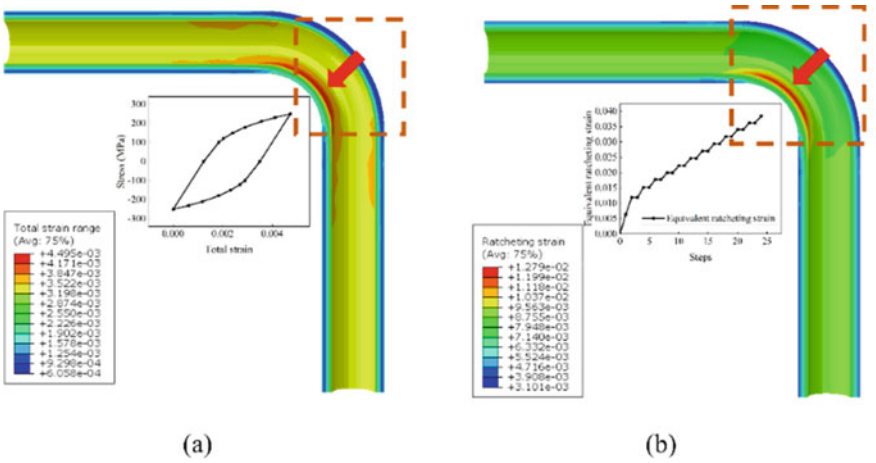

Fig. 11 Typical failure mechanisms in terms of LCF crack initiation and ratcheting for the elbow pipe bend

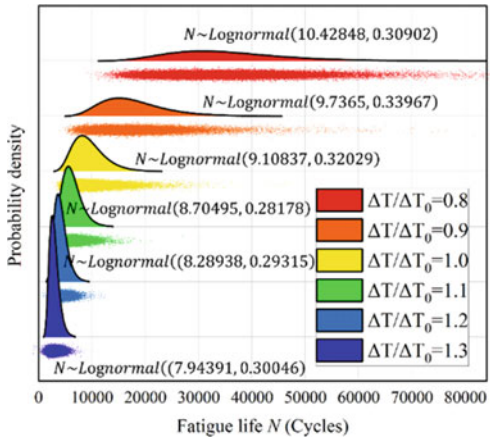

Fig. 12 Statistical distribution of LCF life of the elbow pipe

3.3 Benchmark of Probabilistic Ratcheting Analysis

Probabilistic ratchet limit prediction by LDNN. The probabilistic ratchet limit of the elbow pipe bend is estimated by the LDNN-based surrogate model (with 100 neurons set in the hidden layer) and MCS sampling in terms of the predefined random variables, and the 3D statistical distribution curves are plotted in Fig. 13. Definitely different from the distribution types (Lognormal and Weibull) to depict the probabilistic LCF life, here the probabilistic ratchet limit considering the random variables (including nominal thickness and material property parameters K and n) obey the Normal distribution, with the detailed statistical information provided in Table 4. As

the level of cyclic temperature difference gradually increases, the mean values of the ratchet limit decrease from 79.04 to 69.42 MPa, whereas the standard deviations, accounting for the dispersion degree of the random variable, reduce slightly and remain stable at high-temperature conditions (for the cases where the normalized temperature difference ranges from 1.1 to 1.3).

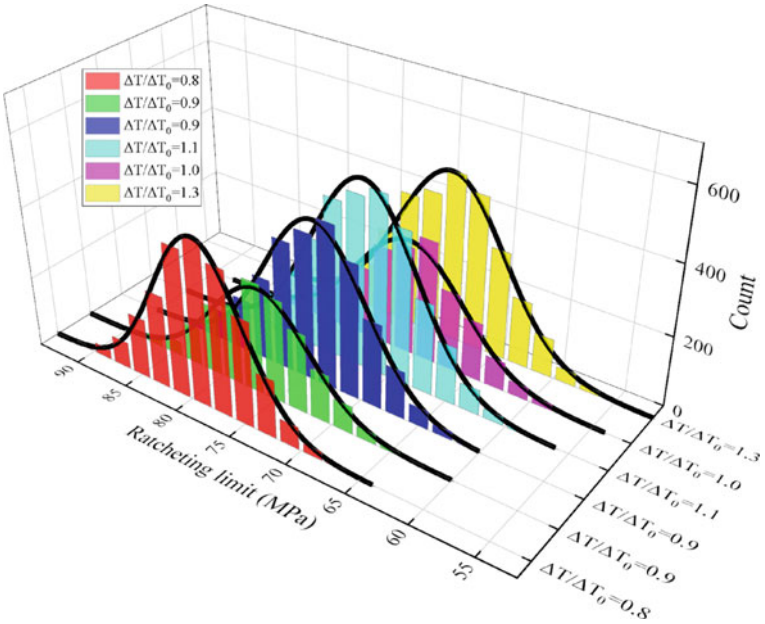

Fig. 13 Statistical distribution of ratchet limit of the elbow pipe under constant inner pressure and various cyclic temperature differences

Table 4 Statistical distribution information of ratchet limit of the elbow pipe under constant inner pressure and various cyclic temperature differences

$\Delta T/\Delta T_0$	Statistical distribution of ratchet limit
0.9	$N \sim Normal$ (76.446, 4.450)
1.0	$N \sim Normal$ (74.162, 4.564)
1.1	$N \sim Normal$ (72.389, 4.667)
1.2	$N \sim Normal$ (70.7137, 4.753)
1.3	$N \sim Normal$(69.416, 4.742)

3.4 Reliability-Based LCF and Ratchet Analyses for the Elbow Pipe Bend

Definition of the unified limit state indicator (ULSI) function. Under the pLMM framework, the unified limit state indicator (ULSI) function is proposed to simplify the subsequent reliability analysis with a concise form by Eq. (6). For the probabilistic LCF life assessment, the LCF multiplier λ_{LCF} in the ULSI function is expressed by the proportion of the predicted structural lifetime to the design life to satisfy the operation requirement (which is predefined as 2,000 cycles in this reliability analysis for the elbow pipe bend). Concerning the probabilistic ratcheting analysis, the ratcheting multiplier $\lambda_{ratcheting}$ is directly generated by the LMM ratcheting procedure, which refers to the amplification factor from the current load level to the ratchet limit when $\lambda_{ratcheting} > 1.0$.

$$\mathbf{G}(\boldsymbol{X}) = \lambda(\boldsymbol{X}) - \mathbf{1} = \begin{cases} \lambda_{LCF}(\boldsymbol{X}) - 1 = \frac{LCF(\boldsymbol{X})}{L_{design}} - 1, & \text{for probabilistic LCF life assessment} \\ \lambda_{ratcheting}(\boldsymbol{X}) - 1, & \text{for probabilistic ratcheting analysis} \end{cases} \tag{6}$$

Reliability-based LCF life and ratchet limit evaluations. Based on the deterministic structural ratcheting boundary in Fig. 10, the load combination located in the reverse plasticity region (in purple colour) is reinvestigated by reliability analysis, where the design parameters are set as random variables. To verify the effectiveness of the pLMM framework, there are two comparison sets employed: the first one is given out by the response surface model (RSM), with the quartic order polynomial leveraged to fit the least-squares regression of the LCF life and the ratchet limit. Another is the step-by-step elastoplastic analysis, during which the LCF life and ratcheting state are determined by either the cyclic plastic strain range or the accumulative plastic strain, respectively. The failure probability regarding a certain cyclic plastic response is calculated via the direct MCS.

The reliability analysis results of the proposed LDNN surrogate model and the RSM-based method are shown in Table 5, with the failure probability compared to the detailed MCS. It can be observed that with the lowest training points involved, the failure probability of the proposed LDNN-based approach is much closer to validation than the RSM-based method for the probabilistic fatigue and ratcheting evaluations. The error generated by the RSM-based method is mainly caused by insufficient training data, which means to guarantee adequate estimation quality, much more training points should be prepared and input during the fitting process of the RSM model.

Table 5 Results of reliability analyses for LCF and ratcheting failures by LDNN surrogate model, RSM model and MCS validation

Failure mode	LDNN-based method		RSM-based method		Verification of MCS with elastoplastic analysis	
	P_f	N_{LDNN}	P_f	N_{RSM}	P_f	N_{MCS}
LCF	0.1048	120	0.1079	250	0.0819	4452
Ratcheting	0.6635	100	0.6802	220	0.6679	4351

Noting that N_{LDNN} and N_{RSM} indicate the gross number of training points used in the training process of the LDNN and RSM surrogate model respectively, and N_{MCS} refers to the total number of elastoplastic simulations during MSC

4 Probabilistic Creep-Fatigue Analysis Under pLMM Framework

4.1 Linear Matching Method-Driven Neural Network (LDNN) for Creep-Fatigue Life Prediction

The probabilistic creep-fatigue assessment under the pLMM framework is performed by using the Linear Matching Method-driven neural network (LDNN), where the basic interpolating function of creep-fatigue lifetime L is given out by Eq. (7). And the numerical implementation process of this proposed probabilistic creep-fatigue analysis is carried out by using the conjunction of ABAQUS and Isight.

$$L(x) = \sum_{i=1}^{N} \beta_i \varphi_i(x) + \beta_{N+1} \tag{7}$$

4.2 Benchmark of Probabilistic Creep-Fatigue Analysis

Random variables in the probabilistic creep-fatigue analysis. In this case study, the same FEA model, the elbow pipe bend operating under a high-temperature environment, is utilized to introduce the applicability of the proposed probabilistic creep-fatigue analysis under the pLMM framework when solving engineering problems. The uncertain design parameters cover the cyclic yield strength $R_{p0.2}(T)$, the creep Norton law coefficients A and n, Nominal thickness t_n, cyclic inner pressure P/P_0, the cyclic temperature difference $\Delta T/\Delta T_0$, and creep dwell time t.

Creep-fatigue failure mechanism of the elbow pipe. Based on the mean values of the design parameters, the typical failure mechanism of the elbow pipe component is plotted in Fig. 14. Due to the effect of geometric discontinuity at the elbow location,

the inner surface of the intrados exhibits the maximum strength of fatigue damage and creep damage simultaneously.

Probabilistic creep-fatigue lifetime prediction. Considering the uncertainty in design parameters of the elbow pipe, the proposed probabilistic creep-fatigue analysis is able to measure the statistical distributions of the creep-fatigue lifetime, as well as the estimation of the statistical information by the proposed LDNN with 120 neurons in the middle layer, as plotted in Fig. 15. The creep-fatigue lifetime follows the log-normal distribution [27], with the logarithmic mean value and the logarithmic standard deviation also fitted.

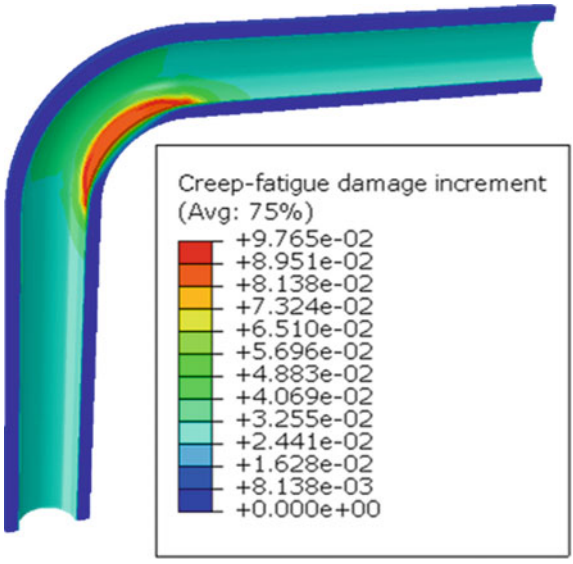

Fig. 14 Creep-fatigue damage increment per cycle of the elbow pipe under the mean values of the design conditions

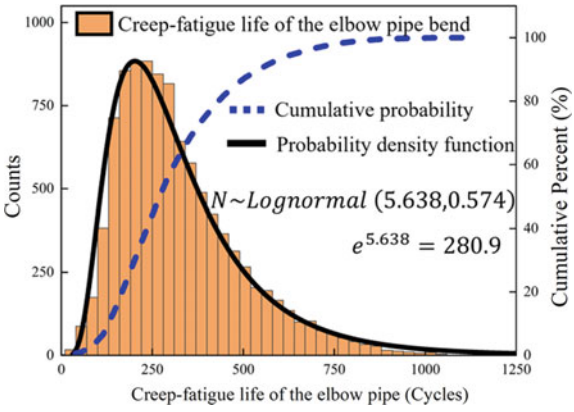

Fig. 15 Statistical distribution of the creep-fatigue responses: **a** damage increment of the elbow pipe; **b** lifetime of the elbow pipe

5 Conclusions

Traditional safety factors are dedicated to pursuing extremely safe designs under uncertain conditions with deterministic assessments, which, inevitably, is an obstacle to achieving precise design and risk management. In this study, a series of probabilistic structural integrity assessment strategies are elaborated under the probabilistic Linear Matching Method (pLMM) framework to consider the uncertainty of the design conditions, where different structural failure behaviours, including shakedown, ratcheting, low cycle fatigue (LCF), and creep-fatigue, are taken into consideration. Detailed benchmarks are also provided, showing the effectiveness and comprehensive applicability of the pLMM framework in engineering problems.

Acknowledgements The authors gratefully acknowledge the support from the National Natural Science Foundation of China (51828501 and 52150710540), the East China University of Science and Technology, and the University of Strathclyde during the course of this work.

References

1. Unfired pressure vessel standard EN 13445, Part 3: Design, Annex B Direct route for design by analysis. European Committee for Standardization (CEN) (2014)
2. Ainsworth RA e. R5: an assessment procedure for the high temperature response of structures. Procedure R5: Issue 3. Gloucester: UK: British Energy Generation Ltd. (2014)
3. ASME. ASME Boiler & Pressure Vessel Code, Section VIII Rules for Construction of Pressure Vessels Division 2, Alternative Rules. The American Society of Mechanical Engineers, New York (2015)
4. Siemaszko, A.: Computational methods for shakedown and limit reliability analysis. Inelastic Behaviour of Structures under Variable Repeated Loads, Springer, Berlin, pp. 345–359 (2002)
5. Heitzer, M., Staat, M.: Structural reliability analysis of elasto-plastic structures. Safety and Reliability AA Balkema, Rotterdam, Brookfield 1999;513:518
6. Staat, M., Heitzer, M.: Part VII probabilistic limit and shakedown problems. Numerical methods for limit and shakedown analysis, 217 (2003)
7. Staat, M.: Limit and shakedown analysis under uncertainty. Int. J. Comp. Meth.-Sing. **11**, 1343008 (2014)
8. Li, X.-Q., Bai, G.-C., Song, L.-K., Wen, J.: Fatigue reliability estimation framework for turbine rotor using multi-agent collaborative modeling. Structures **29**, 1967–1978 (2021)
9. Halfpenny, A., Chabod, A., Czapski, P., Aldred, J., Munson, K., Bonato, M.: Probabilistic fatigue and reliability simulation. Procedia Struct. Integr. **19**, 150–167 (2019)
10. Pierce, S.G., Worden, K., Bezazi, A.: Uncertainty analysis of a neural network used for fatigue lifetime prediction. Mech. Syst. Signal Process. **22**, 1395–1411 (2008)
11. Durodola, J.F., Ramachandra, S., Gerguri, S., Fellows, N.A.: Artificial neural network for random fatigue loading analysis including the effect of mean stress. Int. J. Fatigue **111**, 321–332 (2018)
12. Li, X., Zhang, Y., Abbassi, R., Khan, F., Chen, G.: Probabilistic fatigue failure assessment of free spanning subsea pipeline using dynamic Bayesian network. Ocean. Eng. **234**, 109323 (2021)
13. Mortazavi, S.N.S., Ince, A.: An artificial neural network modeling approach for short and long fatigue crack propagation. Comput. Mater. Sci. **185**, 109962 (2020)

14. Zhang, X.-C., Gong, J.-G., Xuan, F.-Z.: A physics-informed neural network for creep-fatigue life prediction of components at elevated temperatures. Eng. Fract. Mech. **258**, 108130 (2021)
15. Bartošák, M.: Using machine learning to predict lifetime under isothermal low-cycle fatigue and thermo-mechanical fatigue loading. Int. J. Fatigue **163**, 107067 (2022)
16. Chen, H., Chen, W., Li, T., Ure, J.: Shakedown analysis of a composite cylinder with a cross-hole. J. Press. Vessel. Technol. **133** (2011)
17. Chen, H., Ponter, A.R.S.: A direct method on the evaluation of ratchet limit. J. Press. Vessel. Technol. **132** (2010)
18. Chen, Y., Chen, H., Luan, W.: Shakedown, ratcheting and fatigue analysis of cathode coating in lithium-ion battery under steady charging-discharging process. J. Mech. Phys. Solids **150**, 104366 (2021)
19. Cho, N.-K., Wang, R.-Z., Ma, Z., Chen, H., Xuan, F.-Z.: Creep-fatigue endurance of a superheater tube plate under non-isothermal loading and multi-dwell condition. Int. J. Mech. Sci. **161**, 105048 (2019)
20. Wang, X., Ma, Z., Chen, H., Liu, Y., Shi, D., Yang, J.: Creep rupture limit analysis for engineering structures under high-temperature conditions. Int. J. Press. Vessel. Pip. **199**, 104763 (2022)
21. Wang, X., Yang, J., Chen, H., Ma, Z., Xuan, F.: Effect of constraint on cyclic plastic behaviours of cracked bodies and the establishment of unified constraint correlation. Eur. J. Mech.-A/Solids **97**, 104857 (2023)
22. Tran, T.N., Kreissig, R., Staat, M.: Probabilistic limit and shakedown analysis of thin plates and shells. Struct. Saf. **31**, 1–18 (2009)
23. Luo, J., Lin, S., Ni, J., Lei, M.: An improved fingerprint recognition algorithm using EBFNN. In: Proceedings—2nd International Conference on Genetic and Evolutionary Computing, WGEC 2008 (2008)
24. Mak, M.W., Li, C.K.: Elliptical basis function networks and radial basis function networks for speaker verification: a comparative study. In: IJCNN'99 International Joint Conference on Neural Networks Proceedings (Cat. No. 99CH36339), vol. 5, pp. 3034–3039 (1999)
25. Griffiths, G.W., Płociniczak, Ł, Schiesser, W.E.: Analysis of cornea curvature using radial basis functions—part I: methodology. Comput. Biol. Med. **77**, 274–284 (2016)
26. R.M.: Design and Construction rules for Nuclear Power Generating Stations, AFCEN, France (2015)
27. Wang, R., Liu, X., Hu, D., Meng, F., Li, D., Li, B.: Zone-based reliability analysis on fatigue life of GH720Li turbine disk concerning uncertainty quantification. Aerosp. Sci. Technol. **70**, 300–309 (2017)